

Ultrafast dynamics in photo-excited Mott insulator $Sr_3Ir_2O_7$ at high pressure

Xia Yin(尹霞), Jianbo Zhang(张建波), Wang Dong(王东), Takeshi Nakagawa, Chunsheng Xia(夏春生), Caoshun Zhang(张曹顺), Weicheng Guo(郭伟程), Jun Chang(昌峻), and Yang Ding(丁阳)
Citation: Chin. Phys. B, 2024, 33 (**1**): 016103. DOI: 10.1088/1674-1056/acdc8c
Journal homepage: http://cpb.iphy.ac.cn; http://iopscience.iop.org/cpb

What follows is a list of articles you may be interested in

Structural stability and ion migration of Li_2MnO_3 cathode material under high pressures

Ze-Ren Xie(谢泽仁), Si-Si Zhou(周思思), Bei-Bei He(贺贝贝), Huan-Wen Wang(王欢文), Yan-Sheng Gong(公衍生), Jun Jin(金俊), Xiang-Gong Zhang(张祥功), and Rui Wang(汪锐)
Chin. Phys. B, 2023, 32 (**12**): 126101. DOI: 10.1088/1674-1056/ace2b1

Prediction of superionic state in LiH_2 at conditions enroute to nuclear fusion

Fude Li(李福德), Hao Wang(王豪), Jinlong Li(李津龙), and Huayun Geng(耿华运)
Chin. Phys. B, 2023, 32 (**10**): 106103. DOI: 10.1088/1674-1056/acea68

Pressure-induced stable structures and physical properties of Sr-Ge system

Shuai Han(韩帅), Shuai Duan(段帅), Yun-Xian Liu(刘云仙), Chao Wang(王超), Xin Chen(陈欣), Hai-Rui Sun(孙海瑞), and Xiao-Bing Liu(刘晓兵)
Chin. Phys. B, 2023, 32 (**1**): 016101. DOI: 10.1088/1674-1056/ac6db5

Structural evolution and molecular dissociation of H_2S under high pressures

Wen-Ji Shen(沈文吉), Tian-Xiao Liang(梁天笑), Zhao Liu(刘召), Xin Wang(王鑫), De-Fang Duan(段德芳), Hong-Yu Yu(于洪雨), and Tian Cui(崔田)
Chin. Phys. B, 2022, 31 (**7**): 076102. DOI: 10.1088/1674-1056/ac5980

Structural evolution and bandgap modulation of layered β-$GeSe_2$ single crystal under high pressure

Hengli Xie(谢恒立), Jiaxiang Wang(王家祥), Lingrui Wang(王玲瑞), Yong Yan(闫勇), Juan Guo(郭娟), Qilong Gao(高其龙), Mingju Chao(晁明举), Erjun Liang(梁二军), and Xiao Ren(任霄)
Chin. Phys. B, 2022, 31 (**7**): 076101. DOI: 10.1088/1674-1056/ac6db8

SPECIAL TOPIC — States and new effects in nonequilibrium

Ultrafast dynamics in photo-excited Mott insulator $Sr_3Ir_2O_7$ at high pressure

Xia Yin(尹霞)[1], Jianbo Zhang(张建波)[1], Wang Dong(王东)[1], Takeshi Nakagawa[1], Chunsheng Xia(夏春生)[1], Caoshun Zhang(张曹顺)[1], Weicheng Guo(郭伟程)[1], Jun Chang(昌峻)[2,‡], and Yang Ding(丁阳)[1,†]

[1] *Center for High-Pressure Science and Technology Advanced Research, Beijing* 100094, *China*
[2] *College of Physics and Information Technology, Shaanxi Normal University, Xi'an* 710119, *China*

(Received 26 May 2023; revised manuscript received 8 June 2023; accepted manuscript online 8 June 2023)

High-pressure ultrafast dynamics, as a new crossed research direction, are sensitive to subtle non-equilibrium state changes that might be unresolved by equilibrium states measurements, providing crucial information for studying delicate phase transitions caused by complex interactions in Mott insulators. With time-resolved transient reflectivity measurements, we identified the new phases in the spin–orbit Mott insulator $Sr_3Ir_2O_7$ at 300 K that was previously unidentified using conventional approaches such as x-ray diffraction. Significant pressure-dependent variation of the amplitude and lifetime obtained by fitting the reflectivity $\Delta R/R$ reveal the changes of electronic structure caused by lattice distortions, and reflect the critical phenomena of phase transitions. Our findings demonstrate the importance of ultrafast nonequilibrium dynamics under extreme conditions for understanding the phase transition of Mott insulators.

Keywords: ultrafast dynamics, high pressure, phase transition, Mott insulator

PACS: 61.82.Ms, 63.20.kd, 64.60.F–

DOI: 10.1088/1674-1056/acdc8c

1. Introduction

The ultrafast dynamics of non-equilibrium excited states offer direct insight into phase transitions in strongly correlated[1–5] and spin–orbit coupling (SOC) materials,[6–10] both of which are key topics in condensed matter physics. In 5d transition metal compounds, particularly typical Mott insulator $Sr_{n+1}Ir_nO_{3n+1}$ ($n = 1, 2, \infty$), electron–electron correlation and spin–orbit coupling have similar energy scales. They play important roles among all cooperative and strong competing interactions resulting in a remarkable playground for exploring not only novel phases at equilibrium states,[11] but also emergent transient phases and ultrafast dynamics of quasiparticles in non-equilibrium processes.[12] $Sr_{n+1}Ir_nO_{3n+1}$ ($n = 1, 2, \infty$) has attracted much attention due to complex magnetic states at high critical temperature and abnormal insulating states rather than metallic states.[13–17] This narrow-bandgap Mott insulating phase has a complex lattice frustration under high pressure,[18–20] and does not exhibit the expected insulating state collapse and metallization with compression of the unit cell, which has stimulated great interest in tuning the material with pressure.[19–26] However, the ultrafast dynamics of the transient phases in the non-equilibrium region is still less explored at high pressure,[27,28] especially the related research on $Sr_3Ir_2O_7$ has not been published yet.

Recently, several studies have shown that the magnetic and structural transitions of $Sr_3Ir_2O_7$ at high pressure are interdependent. While at 14 GPa in $Sr_3Ir_2O_7$, a magnetic transition occurs at 10 K[20] and a structure transition occurs around 25 K,[29] respectively. Because these two transitions are practically simultaneous, it becomes uncertain whether the magnetic transition is caused by the structural transition or vice versa. According to theoretical modeling,[30] the magnetic transition is triggered by a lattice distortion from a tetragonal IrO_6 octahedral to a cubic IrO_6 octahedral through spin–lattice coupling. To confirm the prediction requests to decouple the magnetic transition and structural transition. One approach is to investigate the lattice distortion above the Néel temperature (285 K)[14] where the magnetic transition is inhibited. Intriguingly, such structural transition observable at room temperature as well as the metal–insulator transition does not occur until 60 GPa,[22,30] possibly because the structure change is too small to be resolved by conventional high-pressure x-ray diffraction and Raman methods. As ultrafast dynamics are sensitive to subtle non-equilibrium state changes, time-resolved studies provide critical information for studying delicate phase transitions at high pressure.

In this work, we investigate the time-resolved differential reflectivity $\Delta R/R$ of $Sr_3Ir_2O_7$ at room temperature and high pressure by combining the pump–probe approach with diamond anvil cells (DAC). Our work has achieved high pressure of 23.2 GPa and *in situ* environment. To minimize the errors caused by removing the sample and DAC from the light path to change and measure the pressure, which is a critical step in the pump–probe transient reflectivity measurements, we

†Corresponding author. E-mail: yang.ding@hpstar.ac.cn
‡Corresponding author. E-mail: junchang@snnu.edu.cn

© 2024 Chinese Physical Society and IOP Publishing Ltd

and colleagues have developed an on-site *in situ* setup.[27,28] We discover that above the Néel temperature, the density and lifetime of quasiparticles (QPs) fluctuate significantly at the transition pressure 14.3 GPa and remain stable in other pressure ranges, indicating the formation of a critical phenomenon. Furthermore, we provide a model that combines quantum interference to account for the crucial behavior near the transition pressure, which provides important information for understanding the phase transition. Our findings suggest that ultrafast non-equilibrium excited states could provide important information for studying phase transitions inaccessible from equilibrium states, and also reveal the potential development prospects for high-pressure ultrafast physics research.

2. Experiments

The 5d transition metal oxide $Sr_{n+1}Ir_nO_{3n+1}$ ($n = 1, 2, \infty$) with typical $J_{\text{eff}} = 1/2$ Mott insulating state has a tetragonal perovskite structure, where n represents the number of Ir–O layers in each unit cell. Electron hopping depends on the overlapping d–d orbitals of Ir ions or/and the p orbitals of oxygen atom, therefore the ground state is exceptionally sensitive to the lattice structure. As n increases, the ground state has narrower charge gap Δ and wider $J_{\text{eff}} = 1/2$ bandwidth, developing from stable insulating phase in Sr_2IrO_4 to weak insulating state in Sr_3IrO_7.[14] Sr_3IrO_7 is at the Mott insulation limit with a charge gap of 0.15 eV[31] and a bandwidth of 0.56 eV.[32] The IrO_6 octahedra in Sr_3IrO_7 has structural distortion with significance for ground state, exhibiting a rotation angle of 11° along the c-axis and a tilt angle of about 1° between the c-axis and the z direction (Fig. 1(a)).[18,33,34] Related reports of Sr_3IrO_7 show that the crystal structure measured from x-ray diffraction is usually stable at $I4/mmm$[35] symmetry, but may be reduced to $Bbca$,[18] $Bbcb$[34] or even $C2/c$.[33] due to the structural distortion. In this work, the single crystal samples were all synthesized by flux technique. High-purity $SrCO_3$, IrO_2 and $SrCl_2{\cdot}6H_2O$ powders were mixed in a certain proportion and kept at high temperature ($\sim$ 1500 K) for several hours. The high-purity single crystal of $0.8\times0.8\times0.3$ mm^3 can be obtained after gradually cooling to room temperature.

We performed the high-pressure time-resolved reflectivity measurements on Sr_3IrO_7 single crystals loaded in Mao–Bell type DAC. The DAC enables a pressurized environment by type-II diamonds with 300 μm culet size, and T301 stainless steel gaskets with 30 μm thickness and 150–170 μm diameter. The selected square sample has a width of 40–50 μm and a thickness of 10 μm. The inert gas neon was used as the pressure transmission medium to achieve a better hydrostatic pressure environment, and the specific pressure was obtained through the ruby fluorescence signal.

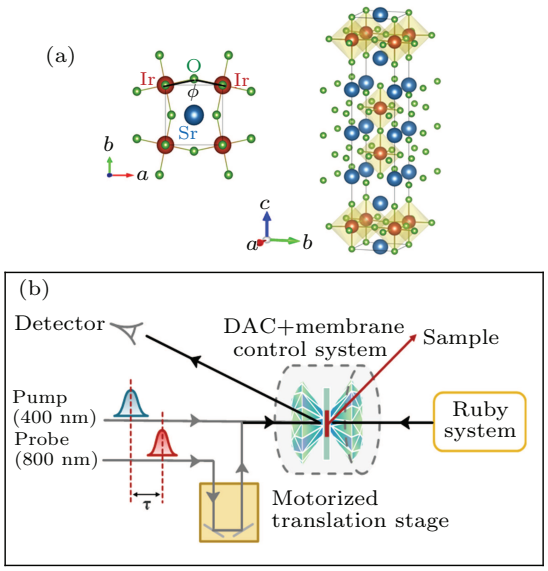


Fig. 1. (a) The lattice structure of $Sr_3Ir_2O_7$, with iridium atoms in red, oxygen atoms in green, and strontium atoms in blue. φ is in-plane rotation angle. (b) The main components of high-pressure pump–probe optical path.

A pump–probe system equipped with a regenerated Ti: sapphire amplifier generates an incident ultrafast pulse laser with a center wavelength of 800 nm, an initial pulse duration of 80 fs, and a repetition rate of 250 kHz. We developed an *in situ* setup to reduce possible measurement artifacts,[28] in which the DAC pressurized using a gas membrane system was kept fixed in the optical path and the pressure was calibrated with an online spectrometer system. The measurement on Sr_3IrO_7 used a 400 nm pump laser beam with a diameter of 4.93 μm ($1/e^2$ beam diameter) and a fluence of 11.89 mJ/cm^2, and a 800 nm probe beam with a diameter of 4.69 μm and a fluence of 2.16 mJ/cm^2. These beams pass through a motorized translation stage to generate a time-dependent optical path difference, which is time-delayed to enable the time-resolved capacities (Fig. 1(b)). The fluences of the pump and probe pulses are linearly dependent on the signal, allowing us to minimize the heating effects. Additionally, the selected data ensures a sufficiently high signal-to-noise ratio, enabling us to acquire high-quality data.

3. Results and discussion

3.1. Time-resolved reflectivity of $Sr_3Ir_2O_7$ at high pressure

We obtained the dynamic process of $Sr_3Ir_2O_7$ at high pressure of 2–23.2 GPa by time-resolved pump–probe reflectivity ($\Delta R/R$) at room temperature. In the pump–probe experiments, a larger pump laser energy was chosen to enhance the intensity of reflection to counteract the possible drop of the signal passing through the DAC, while the probe energy was concentrated near the Fermi surface we are interested in. According to the electronic structure of $Sr_3Ir_2O_7$,[22] the 3.1 eV pump laser pulse excites electrons from the O 2p orbital to

the $J_{\rm eff}=1/2$ upper Hubbard band (UHB) in $Sr_3Ir_2O_7$,[6,36] and the probe laser pulse with an energy of 1.55 eV excites electrons from the $J_{\rm eff}=3/2$ to the $J_{\rm eff}=1/2$ states (inset of Fig. 2). In theory, $\Delta R/R$ is proportional to the QPs density of the photo-excited states,[37,38] and its variation over time reflects the ultrafast relaxation dynamics observed in pump–probe measurements. $\Delta R/R$ shows a rapid positive peak at the initial time ($t=0$ ps) and decays with time, as shown in Fig. 2.

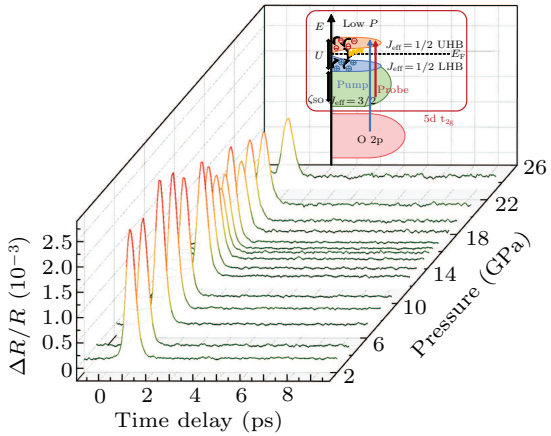


Fig. 2. Time-resolved differential reflectivity $\Delta R/R$ of $Sr_3Ir_2O_7$ in the pressure range of 2–23.2 GPa. The colors of the curve (from green to red) show the strength of $\Delta R/R$ (from low to high). The inset shows the schematic diagram of the low-energy electronic density of states evolving with pressure. The blue arrow indicates the pump pulse with the energy of 3.1 eV, and the red arrow is the probe pulse with the energy of 1.5 eV. The circles with signs are photo-induced holes and electrons.

$Sr_3Ir_2O_7$ exhibits pressure-regulated rotation and tilt distortions, which can have a significant impact on its magnetic and electrical properties due to the strong influence of O 2p orbitals on electronic hopping. Previous studies have identified a structural phase transition driven by lattice frustration at P_c (~ 14 GPa) using x-ray diffraction (XRD).[29] The antiferromagnetic transition and structural phase transition were found to occur simultaneously at P_c,[20] and a several-fold drop in resistivity also occured at this pressure.[30,39] Interestingly, these conclusions were drawn from low-temperature experiments, and neither XRD nor Raman spectroscopy was able to detect the structural transition characteristics at room temperature. The subtle nature of this structural distortion makes it challenging to discern using traditional methods, and its source is difficult to analyze since no symmetry transition is induced. However, despite its subtlety, this transition can cause significant changes in the magnetic and electrical properties, making it a topic of great interest. In our experiments, we have observed that the amplitude of $\Delta R/R$ near $t=0$ ps decreases with increasing pressure, but exhibits a suppression at $P_c=14.3$ GPa, which is in good agreement with the observed transition pressure. This is the first time that high-pressure phase transition signatures in $Sr_3Ir_2O_7$ have been observed by measuring non-equilibrium dynamics at room temperature. The lattice structure transition also affects the electronic structure, as reflected in the non-equilibrium dynamic process, providing us with a research idea to capture the subtle phase transition.

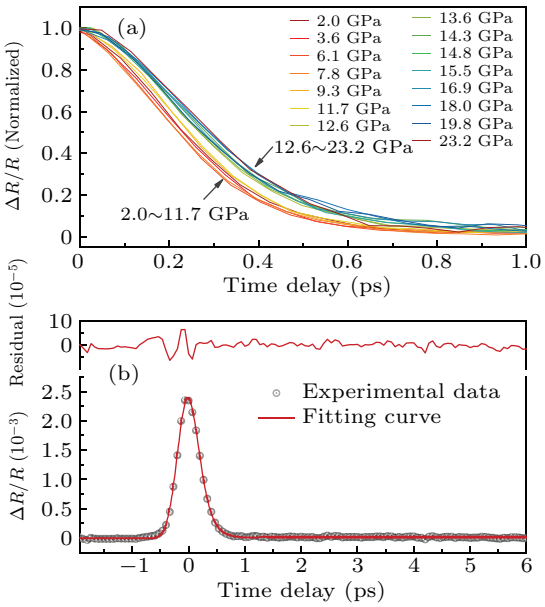


Fig. 3. (a) The normalized results of relative differential reflectivity $\Delta R/R$ of $Sr_3Ir_2O_7$. (b) Schematic of the deconvolution fitting of $\Delta R/R$ at 9.3 GPa. The red solid curve is the fitting result according to the function. Residuals of fitting are shown by the red line above the experimental data.

Phase transitions can also manifest themselves through relaxation processes $\Delta R/R$ ($t>0$). The dynamic behavior of $Sr_3Ir_2O_7$ occurs quite rapidly (in less than 1 ps), possibly due to its narrow energy band gap.[31] Nevertheless, a comparative analysis of the normalized relaxation process reveals distinct dynamic characteristics within the two pressure ranges (Fig. 3(a)). The relaxation process is divided into 2–11.7 GPa and 12.6–23.2 GPa, with the decay becoming slower at higher pressure range. The relaxation frequently involves multiple time-dependent processes, requiring more detailed fitting to determine the details of the phase transitions observed in experiments. Each process can be characterized with two parameters, amplitude A and lifetime τ, by fitting $\Delta R/R$ in exponential function. In our measurements, the output signal results from a convolution of the resolution function with the response function from the samples. Peak fitting and deconvolution techniques are commonly used to resolve the time response from samples. Fitting $\Delta R/R$ to the convolution function accomplishes this,[5,9]

$$[f\otimes g](t)\equiv\int_{-\infty}^{\infty}f(\xi)\,g(t-\xi)\,\mathrm{d}\xi, \tag{1}$$

where the exponential function $f(t)=A\exp(-t/\tau)+A_0$ (A_0 is the time-independent component) and $g(t)$ is the Gaussian function. The fitted half-width of the Gaussian function is 160 fs, which correlates to the laser pulse. The fitted image

and raw data are shown in Fig. 3(b), with error bar reflected by the residual that is 1–2 orders smaller than the experimental result (see Appendix B for detailed fitting process). Through deconvolution fitting, the data reflecting the real dynamic process in the experimental results can be more accurately separated, consequently, a clearer and more refined physical image can be extracted.

3.2. Critical anomalies of dynamic parameters at P_c

$Sr_3Ir_2O_7$ usually has two relaxation components at low temperatures.[9] At room temperature, the fitting yields only one process characterized by parameters A, τ and A_0 (Figs. 4(a)–4(c)). R, exclusively excited by the probing laser, exhibits a uniform linear relationship (Fig. 4(d)), indicating that the critical dynamics reflect sample characteristics rather than being influenced by the background. The linear decrease of R under high pressure may be affected by diamond window or pressure transmission medium on pulsed laser under high pressure, and the influence of this problem on the signal can be reduced by $\Delta R/R$ processing. We discovered that the density A and lifetime τ of quasiparticles (QPs) vary significantly at P_c, indicating an unusual electrodynamic signature.

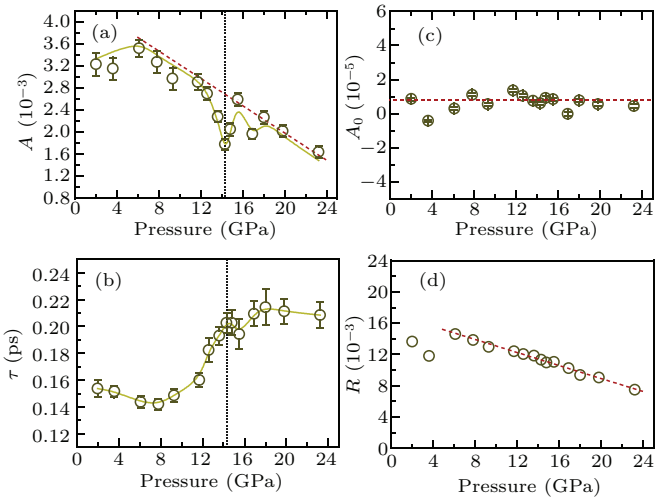


Fig. 4. Pressure dependence of the (a) amplitude A, (b) lifetime τ and (c) constant A_0 in $Sr_3Ir_2O_7$. (d) The experimentally measured R when only the probe laser is used for excitation. It is relatively stable at high pressure and proves that there is indeed a critical fluctuation. The vertical dotted lines mark the phase transition pressure, and the green curves in (a), (b) and red dotted lines in (a), (c), (d) represent the trend guide of points.

Overall, A decreases linearly with pressure, but there is a noticeable dip near critical pressure and rapidly reaches a minimum at P_c. In this pressure range, τ rapidly increases from 0.15 ps to 0.22 ps, also forming a small peak at 14.3 GPa. This type of fluctuation distinguishes a crucial phenomenon from the rest of the pressure range. According to the pressure dependence of A and τ, the phase space can be divided into three regions: phase I ($< P_c$), a critical region around P_c, and phase II ($> P_c$). Simultaneously, it can be considered that time-independent component A_0 fluctuates around a relatively stable constant value at high pressure. The following discussion will focus on the phenomena observed in A and τ.

According to the Fermi gold rule,[40] the amplitude A in the photoexcited system is dominated by the joint electron density of states between the O 2p band and the $J_{\text{eff}} = 1/2$ UHB, and the successive decrease of A with pressure reflects the increases in bandwidth due to compression. Given that the O 2p band is commonly wider than the $J_{\text{eff}} = 1/2$ UHB, it is expected that the broadening of the O 2p band will play a dominant role in the change of A, which is not very sensitive to small change of the IrO_6 octahedral. As pressure-induced increase in bandwidth is common, a decrease in the amplitude A with pressure at the non-phase transition point is also frequently observed in some high-pressure studies.[27,41] Another possibility is that the pulse signal is weakened by the diamond window and the pressure medium at high pressure. However, none of the above can explain the problem of fluctuations in the critical pressure point P_c observed in A.

The fast decay component (as shown in Fig. 4(b)) less than 1 ps is widely thought to reflect electron–phonon scattering,[27,28] which is usually difficult to change by external temperature or pressure modulation, and also generally manifested a constant in ultrafast experiments.[42] The τ obtained in this experiment remains stable in phases I and II, but exhibits some critical pressure dependence, such as a rapid rise near the P_c.

The anomalies observed in the ultrafast dynamics have important implications for the study of difficult-to-metallize properties and associated phase transitions at high pressures. First-principles calculations[30] predict that the 0.15 eV band gap in $Sr_3Ir_2O_7$ will be closed at 20 GPa due to volume-reduction-induced bandwidth broadening,[30,39] while up to 60 GPa, $Sr_3Ir_2O_7$ still does not exhibit full metallization.[22,30] This is due to $Sr_3Ir_2O_7$'s remarkable lattice frustration, which is caused by the spin–orbital coupling presenting in the interplay of the lattice, orbital, spin, and charge.[14,20,22,29,43,44] In previous work, structural phase transitions at $\sim$ 14 GPa were often accompanied by changes in conductivity and magnetism,[20,29,39] and such strong correlations could not be separated. However, the critical anomaly observed in this study coincides well with the phase transition pressure P_c and occurs at room temperature (above the Néel temperature 285 K of paramagnetic–antiferromagnetic transition point), which can clearly rule out the influence of the magnetic order phase transition. Therefore, the observed rapid increase in the quasiparticle (QP) lifetime τ at P_c can be attributed to the abundance of lattice distortions in iridium oxides. Theoretical models suggest that high pressure may induce lattice distortion from tetragonal IrO_6 octahedra to cubic IrO_6 octahedra,[30] and some experiments have found that variations in the rotational angles within the Ir–O–Ir plane[20] or the tilting an-

gles outside the plane[45] may affect the band structure. These lattice distortions of IrO_6 octahedra will affect the distribution of O 2p orbitals and overlap of d–d orbitals,[14] leading to hybridization of t_{2g} orbitals and affecting electron hopping, which can result in changes in electron–phonon interaction and/or band gap, and reflected in the dynamic lifetime τ. In any case, it is obvious that we observed an anomaly in the nonequilibrium dynamics at phase transition pressure through the analysis of the QPs density and lifetime.

3.3. Critical phenomena model

The fluctuations in density A and lifetime τ around P_c can also be explained by critical phenomena. The non-equilibrium critical slowing is universally observed at the charge density wave or superconducting transition temperature,[46] however, similar fluctuations near the critical points of other phase transition mechanisms repeatedly found in ultrafast experiments are still poorly understood.[1,27,41,47] In the following section, we use a model to account for the universal temporal behavior of the photoexcited states forming around the phase transition point of the phase transition.

According to Landau phase-transition theory based on the free energy of equilibrium ground states, the well-known critical slowing down or the lifetime divergence under perturbation can clearly be observed at a continuous phase transition point. However, the photoexcited states are far from the equilibrium states and our experiment's relaxation-time enhancement is relatively weak. More remarkably, in some other experiments, the relaxation time even is strongly shortened at the phase transition point,[3,27] in contrary to the expectation of the critical slowing down. In addition, the density of the photoinduced QPs shows a dip near the critical pressure but almost linearly depends on the pressure in other pressure regimes. A parameter change that is induced by the phase transition is supposed to give rise to a step function-like response for the density. Therefore, a new model is expected to explain the anomaly around the phase-transition point. The anomalous phenomenology of dynamics near a phase transition point is much more general in first and second order phase transitions, glasses and dynamical systems.[48] Here, we propose a phenomenological model to study the time evolution of the photoexcited states near the phase-transition points, as shown in Fig. 5. We assume that ψ_1 and ψ_2 are the wave functions of the excited states in the neighboring phases I or II, respectively. At the phase-transition point, two excited states coexist and weakly couple. The quantum coherence is set up by "tunneling" between the two excited states. Mimicking Feynman's phenomenological model of the Josephson junction,[49,50] the time evolutions of the two coupling wave functions of the excited states are written as

$$i\hbar\frac{\partial\psi_1}{\partial t} = (U_1 - i\Gamma_1)\,\psi_1 + \left(K - iK'\right)\psi_2, \tag{2}$$

$$i\hbar\frac{\partial\psi_2}{\partial t} = (U_2 - i\Gamma_2)\,\psi_2 + \left(K - iK'\right)\psi_1, \tag{3}$$

where U_1, U_2 and Γ_1, Γ_2 are the energies and the relaxation rates of the two excited states, respectively. K and K' are the state coupling constant and relaxation rate constant, respectively. If K and K' are zero, then the two Schrödinger equations only describe the two respective excited states. Near the phase transition point, the coupling or fluctuation between the two states may induce tunneling from one state to the other. Following Feynman's method, we define the wave functions as $\psi_1 = \sqrt{\rho}_1\,e^{i\theta_1}$, $\psi_2 = \sqrt{\rho}_2\,e^{i\theta_2}$, where θ_1 and θ_2 are the phases of the two wave functions, respectively, and ρ_1 and ρ_2 the corresponding densities of the QPs of the two excited states. Substituting the above equations into the Schrödinger equations, one gets

$$\hbar\frac{\partial\rho_1}{\partial t} = -2\Gamma_1\rho_1 + 2K\sqrt{\rho_1\rho_2}\sin\delta - 2K'\sqrt{\rho_1\rho_2}\cos\delta, \tag{4}$$

with the phase difference $\delta = \theta_2 - \theta_1$. We further define the total excited QPs density as $\rho = \rho_1 + \rho_2$, giving $\hbar\partial\rho/\partial t = -2\Gamma'\rho$ with the effective relaxation rate

$$\Gamma' = \Gamma_1\frac{\rho_1}{\rho} + \Gamma_2\frac{\rho_2}{\rho} + 2K'\frac{\sqrt{\rho_1\rho_2}}{\rho}\cos\delta. \tag{5}$$

We assume $\Gamma_1 \approx \Gamma_2 = \Gamma$ when only considering the phase-transition point; then, the effective relaxation rate reads

$$\Gamma' = \left(1 + \frac{2\sqrt{\rho_1\rho_2}K'\cos\delta}{\rho\Gamma}\right)\Gamma. \tag{6}$$

Since $0 \le 2\sqrt{\rho_1\rho_2}/\rho \le 1$, the relaxation rate Γ' at the phase-transition point is not equal to Γ unless the phase difference is $\delta = \pi/2$ or $3\pi/2$. Furthermore, when $\rho_1 = \rho_2$ and $K' = \Gamma$, one finds $\Gamma' = (1+\cos\delta)\,\Gamma$. Therefore, the lifetime anomaly at the phase-transition point could result from the interference between the two coexisting excited states in neighboring phases, the phase difference δ could be associated with the electron–phonon coupling changes caused by the lattice distortion. But the underlying microscopic mechanism still remains to be explored.

This model could also explain the prominent dip in amplitude A of the QPs at the phase transition point (Fig. 4(a)). The amplitude of the QPs $A \sim \rho_O\bar{\rho}_e$, where ρ_O is the density of the electrons in the O 2p band, and $\bar{\rho}_e$ is the unoccupied density of the QPs in the photoexcited states. Near the phase-transition point, two phase states coexist, and the amplitude of the QPs is $A \sim \rho_{1O}\bar{\rho}_{1e} + \rho_{2O}\bar{\rho}_{2e}$. We assume $\rho_O = \rho_{1O} + \rho_{2O}$ and $\bar{\rho}_e = \bar{\rho}_{1e} + \bar{\rho}_{2e}$, giving $\frac{\rho_O\bar{\rho}_e}{2} \le \rho_{1O}\bar{\rho}_{1e} + \rho_{2O}\bar{\rho}_{2e} \le \rho_O\bar{\rho}_e$. Here, we assumed that the electrons in phase I (II) could not be excited to the photoexcited state in phase II (I). When the system locates in single phase I or II near the critical pressure, we assume $\rho_{1O} \approx \rho_{2O} \approx \rho_O$ and $\bar{\rho}_{1e} \approx \bar{\rho}_{2e} \approx \bar{\rho}_e$. Consequently, according to the results of our critical model, the population of the photoexcited QPs always decreases to less than half around the phase-transition point.

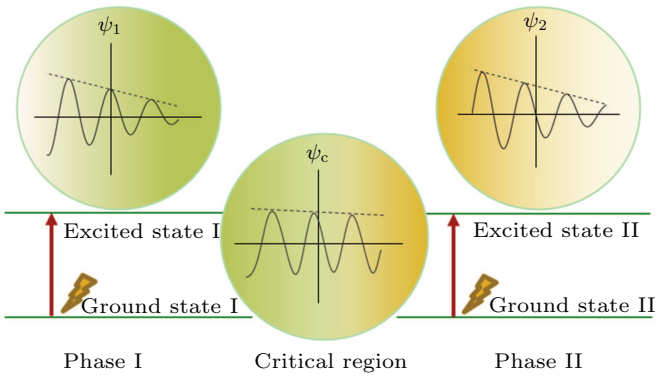


Fig. 5. Schematic of critical point model demonstrating interference between two excited states belonging to two neighboring phases. The wave figures show the real (imaginary) part of the wave functions $\psi_1 = \sqrt{\rho}_1 e^{i\theta_1}$ in phase I, $\psi_2 = \sqrt{\rho}_2 e^{i\theta_2}$ in phase II and ψ_c in the critical region. The ground state I, II and the excited state I, II could coexist together and the relaxation time could be far from that in phase I and II in the critical region.

4. Conclusion and perspectives

In summary, we investigated the ultrafast dynamics in photo-excited $Sr_3Ir_2O_7$ under high pressures at 300 K by applying *in situ* time-resolved differential spectroscopy. The density and lifetime of QPs vary widely at $P_c = 14.3$ GPa, evincing the lattice phase transition induces significant changes in the transient dynamics. Furthermore, we propose a model that accounts for the crucial behavior near the transition pressure point. The ability to reveal novel phase from its distinct non-equilibrium states demonstrated in this study gives a new way to investigate more delicate phases at high pressure, which are unresolvable by standard x-ray diffraction and Raman spectroscopy. Since non-equilibrium dynamics involves many influencing factors, we need further experimental or computational support to explain the observed physical phenomena at high pressure clearly. For example, if the correlation between structural transformation and electroacoustic coupling can be clarified, the lifetime difference between two phases at high pressure can be well explained by electron–phonon coupling alone without introducing other considerations. In any case, paying attention to non-equilibrium state under high pressure will provide a new perspective for the study of condensed matter physics and help people solve some long-standing problems.

Appendix A: The trajectories of Gaussian function and exponential function fittings

In the measurements, the output signal is resulted from a convolution of the temporal resolution function of the instrument with the temporal response function from the materials. To resolve the time response from samples, one needs to apply peak fitting and deconvolution techniques, the precision of such analysis is typically about 1/10 of the temporal resolution of the experiment, which in this study is about 8–10 fs. Figure A1 shows the analysis. It can be observed that using deconvolution fitting reveals the true relaxation dynamics process (green curve), while neglecting this treatment would mask this information.

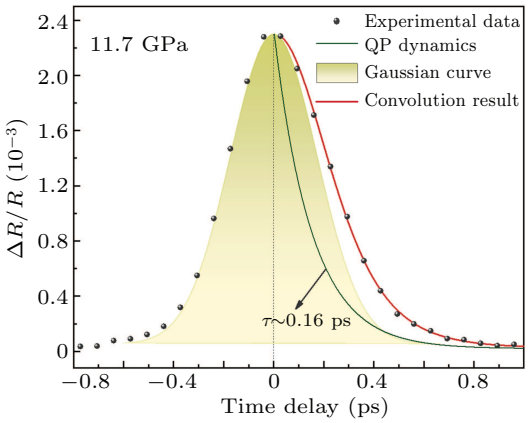


Fig. A1. Deconvolution of the QP dynamics in $Sr_3Ir_2O_7$.

Appendix B: Deconvolution fitting of high pressure time-resolved dynamics

In this study, carefully fitting the dynamic spectra under high pressure was performed, as shown in the comparison between the deconvolution fitting results and the original data of the differential reflectivity $\Delta R/R$. The peak shape of the differential reflectivity can be well fitted, and the relaxation parameters obtained from the fitting above 0 ps accurately reflect the dynamic processes of the experimental data.

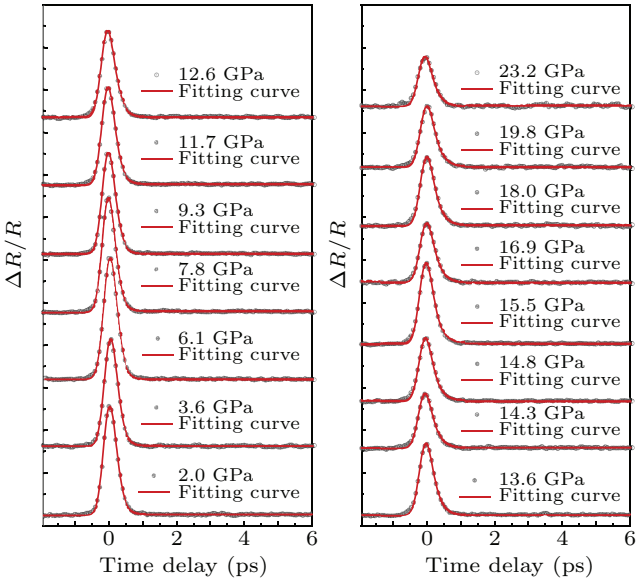


Fig. B1. Raw data and deconvolution fitting results of each high-pressure ultrafast dynamic spectrum in the pressure range of 2–23.5 GPa.

Acknowledgements

The project supported by the National Key Research and Development Program of China (Grant

No. 2018YFA0305703), Science Challenge Project (Grant No. TZ2016001), and the National Natural Science Foundation of China (Grant Nos. U1930401 and 11874075).

References

[1] Hsieh D, Mahmood F, Torchinsky D H, Cao G and Gedik N 2012 *Phys. Rev. B* **86** 035128

[2] Orenstein J 2012 *Phys. Today* **65** 44

[3] Tian Y C, Zhang W H, Li F S, Wu Y L, Wu Q, Sun F, Zhou G Y, Wang L, Ma X, Xue Q K and Zhao J 2016 *Phys. Rev. Lett.* **116** 107001

[4] Demsar J, Podobnik B, Kabanov V, Wolf T and Mihailovic D 1999 *Phys. Rev. Lett.* **82** 4918

[5] Wu Q, Zhou H, Wu Y, Hu L, Ni S, Tian Y, Sun F, Zhou F, Dong X and Zhao Z 2020 *Chin. Phys. Lett.* **37** 097802

[6] Afanasiev D, Gatilova A, Groenendijk D, Ivanov B, Gibert M, Gariglio S, Mentink J, Li J, Dasari N and Eckstein M 2019 *Phys. Rev. X* **9** 021020

[7] Krauß M, Aeschlimann M and Schneider H C 2008 *Phys. Rev. Lett.* **100** 256601

[8] Wragg J, Clarke D D, Armstrong G S, Brown A C, Ballance C P and Van Der Hart H W 2019 *Phys. Rev. Lett.* **123** 163001

[9] Hu L, Yang M, Wu Y, Wu Q, Zhao H, Sun F, Wang W, He R, He S and Zhang H 2019 *Phys. Rev. B* **99** 094307

[10] Huang Y, Zhao H, Li Z, Hu L, Wu Y, Sun F, Meng S and Zhao J 2023 *Advanced Materials* **35** 2208362

[11] Jackeli G and Khaliullin G 2009 *Phys. Rev. Lett.* **102** 017205

[12] Alpichshev Z, Mahmood F, Cao G and Gedik N 2015 *Phys. Rev. Lett.* **114** 017203

[13] Cao G, Bolivar J, McCall S, Crow J and Guertin R 1998 *Phys. Rev. B* **57** R11039(R)

[14] Cao G and Schlottmann P 2018 *Rep. Prog. Phys.* **81** 042502

[15] Cava R J, Batlogg B, Kiyono K, Takagi H, Krajewski J J, Peck W F Jr., Rupp L W, Jr. and Chen C H 1994 *Phys. Rev. B* **49** 11890

[16] Crawford M, Subramanian M, Harlow R, Fernandez-Baca J, Wang Z and Johnston D 1994 *Phys. Rev. B* **49** 9198

[17] Huang Q, Soubeyroux J, Chmaissem O, Sora I N, Santoro A, Cava R, Krajewski J and Peck Jr W 1994 *J. Phys. Condens. Matter* **112** 355

[18] Cao G, Xin Y, Alexander C S, Crow J E, Schlottmann P, Crawford M K, Harlow R L and Marshall W 2002 *Phys. Rev. B* **66** 214412

[19] Hogan T, Yamani Z, Walkup D, Chen X, Dally R, Ward T Z, Dean M P, Hill J, Islam Z, Madhavan V and Wilson S D 2015 *Phys. Rev. Lett.* **114** 257203

[20] Zhang J, Yan D, Yesudhas S, Deng H, Xiao H, Chen B, Sereika R, Yin X, Yi C, Shi Y, Liu Z, Pärschke E M, Chen C C, Chang J, Ding Y and Mao H K 2019 *npj Quantum Mater.* **4** 1

[21] de la Torre A, Hunter E C, Subedi A, McKeown Walker S, Tamai A, Kim T K, Hoesch M, Perry R S, Georges A and Baumberger F 2014 *Phys. Rev. Lett.* **113** 256402

[22] Ding Y, Yang L, Chen C C, Kim H S, Han M J, Luo W, Feng Z, Upton M, Casa D, Kim J, Gog T, Zeng Z, Cao G, Mao H K and van Veenendaal M 2016 *Phys. Rev. Lett.* **116** 216402

[23] Gretarsson H, Sung N H, Hoppner M, Kim B J, Keimer B and Le Tacon M 2016 *Phys. Rev. Lett.* **116** 136401

[24] Kim J, Said A H, Casa D, Upton M H, Gog T, Daghofer M, Jackeli G, van den Brink J, Khaliullin G and Kim B J 2012 *Phys. Rev. Lett.* **109** 157402

[25] Kim J W, Choi Y, Kim J, Mitchell J F, Jackeli G, Daghofer M, van den Brink J, Khaliullin G and Kim B J 2012 *Phys. Rev. Lett.* **109** 037204

[26] Lu X, McNally D E, Moretti Sala M, Terzic J, Upton M H, Casa D, Ingold G, Cao G and Schmitt T 2017 *Phys. Rev. Lett.* **118** 027202

[27] Wu Y, Yin X, Hasaien J, Ding Y and Zhao J 2020 *Chin. Phys. Lett.* **37** 047801

[28] Wu Y, Yin X, Hasaien J, Tian Z, Ding Y and Zhao J 2021 *Rev. Sci. Instrum.* **92** 113002

[29] Zhao Z, Wang S, Qi T F, Zeng Q, Hirai S, Kong P P, Li L, Park C, Yuan S J, Jin C Q, Cao G and Mao W L 2014 *J. Phys. Condens. Matter* **26** 215402

[30] Donnerer C, Feng Z, Vale J G, Andreev S N, Solovyev I V, Hunter E C, Hanfland M, Perry R S, Rønnow H M, McMahon M I, Mazurenko V V and McMorrow D 2016 *Phys. Rev. B* **93** 174118

[31] Fujiyama S, Ohashi K, Ohsumi H, Sugimoto K, Takayama T, Komesu T, Takata M, Arima T and Takagi H 2012 *Phys. Rev. B* **86** 174414

[32] Moon S, Jin H, Kim K W, Choi W, Lee Y, Yu J, Cao G, Sumi A, Funakubo H and Bernhard C 2008 *Phys. Rev. Lett.* **101** 226402

[33] Hogan T, Bjaalie L, Zhao L, Belvin C, Wang X, Van de Walle C G, Hsieh D and Wilson S D 2016 *Phys. Rev. B* **93** 134110

[34] Matsuhata H, Nagai I, Yoshida Y, Hara S, Ikeda S I and Shirakawa N 2004 *J. Solid State Chem.* **177** 3776

[35] Subramanian M, Crawford M and Harlow R 1994 *Mater. Res. Bull.* **29** 645

[36] Ishii K, Jarrige I, Yoshida M, Ikeuchi K, Mizuki J, Ohashi K, Takayama T, Matsuno J and Takagi H 2011 *Phys. Rev. B* **83** 115121

[37] Kabanov V, Demsar J, Podobnik B and Mihailovic D 1999 *Phys. Rev. B* **59** 1497

[38] Torchinsky D H, Chen G F, Luo J L, Wang N L and Gedik N 2010 *Phys. Rev. Lett.* **105** 027005

[39] Li L, Kong P P, Qi T F, Jin C Q, Yuan S J, DeLong L E, Schlottmann P and Cao G 2013 *Phys. Rev. B* **87** 235127

[40] Bransden B H and Joachain C J 1989 *Introduction to quantum mechanics* (United Kingdom: Longman Scientific and Technical), p. 70, ISBN 0-582-44498-5

[41] Zhang K, Jiang H, Yang J, Zhang J, Zeng Z, Chen X and Su F 2020 *Appl. Phys. Lett.* **117** 101105

[42] Giannetti C, Capone M, Fausti D, Fabrizio M, Parmigiani F and Mihailovic D 2016 *Adv. Phys.* **65** 58

[43] Rau J G, Lee E K H and Kee H Y 2016 *Annu. Rev. Condens. Matter Phys.* **7** 195

[44] Witczak-Krempa W, Chen G, Kim Y B and Balents L 2014 *Annu. Rev. Condens. Matter Phys.* **5** 57

[45] Nie Y F, King P, Kim C, Uchida M, Wei H, Faeth B D, Ruf J, Ruff J, Xie L and Pan X 2015 *Phys. Rev. Lett.* **114** 016401

[46] Rothwarf A and Taylor B N 1967 *Phys. Rev. Lett.* **19** 27

[47] An Y Q, Taylor A J, Conradson S D, Trugman S A, Durakiewicz T and Rodriguez G 2011 *Phys. Rev. Lett.* **106** 207402

[48] Zong A, Dolgirev P E, Kogar A, Ergeçen E, Yilmaz M B, Bie Y Q, Rohwer T, Tung I C, Straquadine J and Wang X 2019 *Phys. Rev. Lett.* **123** 097601

[49] Martinis J M, Devoret M H and Clarke J 2020 *Nat. Phys.* **16** 234

[50] Zhang J Y, Yin X, Liu M Y, Zhao J, Ding Y and Chang J 2023 *Phys. Scripta* **98** 055927